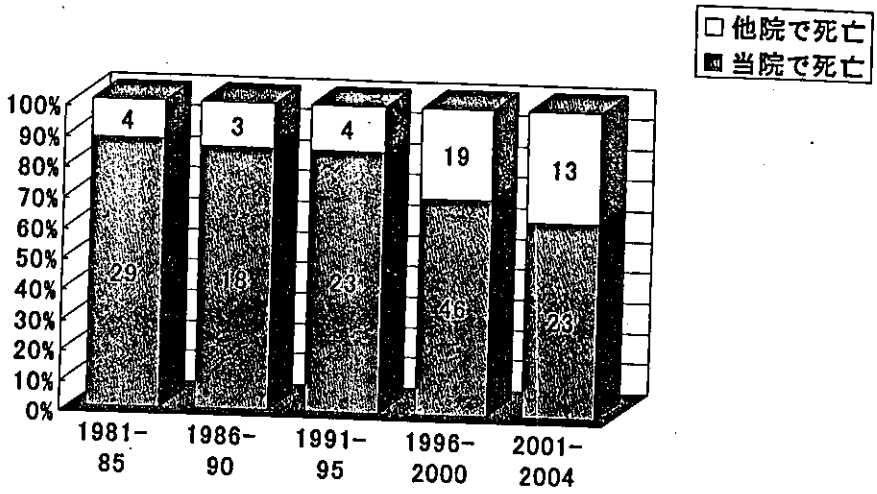

Figure 7. 死亡場所別年次推移

護師・ソーシャルワーカーがお受けしています。ご家族からの相談にも対応しています。また、患者さんやご家族が、がんとその関連情報(患者会、福祉サービス等)を調べることができるように情報コーナーも設置しています。このように医療連携室では、当院をいかに円滑に利用していただくかということに限らず、退院後の支援を含めて広範囲な対応を行っている。また当院医療連携室の推奨する早い段階からの関わり[2]を実践するために脳神経外科では医療連携室での脳神経外科担当者に毎週定期的に来棟してもらい、個別に情報交換を行うとともに、在宅療養への準備を含めた後方支援が必要と思われる患者家族には早期に面談の機会を設けており、円滑な退院、転院の準備も行っている。ただし調査結果でも分かる通り、その利用状況は年々増加してきており、現状ではこの医療連携室の仕事はかなりの過剰労働となっているのが現実である。今後ともこの医療連携室のように医療を側面から援助する機能が必須であることは言うに及ばず、特定機能の医療をより高度に担うことが医療行政のみならず一般の方々からも要求されている現在、さらに終末期医療と表裏一体の疾患を扱う当院ではなおのことその役割はより重要になると考える。

悪性脳腫瘍患者の治療を行う施設として、その延長線上にある終末期をどのような状態で、どこで行うかは、医療者だけでなく患者および家族にとっても非常に深刻な問題の一つである。さらに医師を含めた在宅医療を担当する者が、脳腫瘍という特殊な病態を十分に理解し対処することが難しいことも[1]この問題をより複雑としている。患者家族は個々に在宅介護の努力を行ってはいるが、それには限界があり時期の違いはあるものの医療機関への依存は避けられないところである。一方で当院へ入院となった神経膠腫患者の死亡場所別の調査結果や死亡場所別の推移をみると、当院で継続して終末期を迎えることの困難さが反映された結果となっている。現実の問題として治療開始の病院で終末期から死亡へと移行することは徐々に困難となってきており、ある程度の機能を各病院が分担せざるを得ない時代となってきているのは否定できないところである。すなわち手術治療を含めた高度医療の集中化や、特定機能病院での専門医療の推進がなされていくなかで、全ての医療行為を一つの医療施設で継続することはもはやできなくなってきている。だからといって全ての患者を後方病院に依頼することもまた不可能なことであり、このような状況も考慮すると先述の医療相談や医療連携室が担う役割は今後ともさらに大きくなると思われる。しかしこれに加えてなおわれわれが努力すべきことの一つとして、外来診療からはじまる一連の医療行為において、治療内容に限らずこれらの内容も含めたより十分な説明と納得の上で医療を行っていくことが重要で求められていくところと考える。

【文 献】

1) 田島正孝：グリオブラストーマの在宅末期医療. No Shinkei Geka 27：291, 1999
2) 大松重宏：がん専門病院における医療連携室. がん患者と対処療法13：58-61, 2002

GTS

Fluorine 18–tagged fluorodeoxyglucose positron emission tomographic scanning to predict lymph node metastasis, invasiveness, or both, in clinical T1 N0 M0 lung adenocarcinoma

Hiroaki Nomori, MD, PhD[a]
Kenichi Watanabe, MD[a]
Takashi Ohtsuka, MD[a]
Tsuguo Naruke, MD, PhD[a]
Keiichi Suemasu, MD, PhD[a]
Toshiaki Kobayashi, MD, PhD[b]
Kimiichi Uno, MD, PhD[c]

See related editorial on page 341.

Objective: We sought to predict lymph node metastasis and tumor invasiveness in clinical T1 N0 M0 lung adenocarcinomas, and we measured fluorodeoxyglucose uptake on positron emission tomography.

Methods: Fluorodeoxyglucose positron emission tomography was performed on 44 patients with adenocarcinomas of 1 to 3 cm in size clinically staged as T1 N0 M0 before major lung resection with lymph node dissection. Fluorodeoxyglucose uptake was evaluated by using the contrast ratio between the tumor and contralateral healthy lung tissue. Lymphatic and vascular invasion within tumors, pleural involvement, and grade of histologic differentiation were examined.

Results: The pathologic tumor stage was T1 N0 M0 in 36 patients, and a more advanced stage was found in 8 patients. Although all 22 adenocarcinomas with a contrast ratio of less than 0.5 in fluorodeoxyglucose uptake were pathologic T1 N0 M0 tumors, 8 (36%) of 22 with a contrast ratio of 0.5 or greater were of a more advanced stage than T1 N0 M0, with the difference being significant ($P = .002$). Adenocarcinomas with a contrast ratio of less than 0.5 showed less lymphatic and vascular invasion and less pleural involvement than those with a contrast ratio of 0.5 or greater ($P = .006$, $P = .004$, and $P = .02$, respectively). The grade of histologic differentiation was well differentiated in 19 of 22 adenocarcinomas with a contrast ratio of less than 0.5 (86%), which was a greater frequency than the 4 (18%) of 22 adenocarcinomas with a contrast ratio of 0.5 or greater ($P < .001$).

Conclusion: Clinical T1 N0 M0 lung adenocarcinomas with a contrast ratio of less than 0.5 usually did not have lymph node metastasis, had less tumor involvement of vessels or pleura, and were more frequently well differentiated than those with a contrast ratio of 0.5 or greater. Limited lung resection could be indicated, lymph node dissection or mediastinoscopy could be reduced, or both in this type of adenocarcinoma.

From the Department of Thoracic Surgery,[a] Saiseikai Central Hospital, Tokyo, Japan; the Endoscopy Division,[b] National Cancer Center Hospital, Tokyo, Japan; and Nishidai Clinic,[c] Tokyo, Japan.

This work was supported in part by a Grant-in-Aid from the Ministry of Health, Labor, and Welfare of Japan.

Received for publication Dec 17, 2003; revisions requested Feb 12, 2004; accepted for publication March 22, 2004.

Address for reprints: Hiroaki Nomori, MD, PhD, Department of Thoracic Surgery, Saiseikai Central Hospital, 1-4-17 Mita, Minato-ku, Tokyo 108-0073, Japan (E-mail: hnomori@qk9.so-net.ne.jp).

J Thorac Cardiovasc Surg 2004;128:396-401

0022-5223/$30.00

doi:10.1016/j.jtcvs.2004.03.020

Recent advances in low-dose helical computed tomography (CT) and video-assisted thoracoscopic surgery have enabled the diagnosis of lung cancers while still small in size.[1-6] Although limited resection procedures, such as lung wedge resection or segmentectomy, can cure some clinical T1 N0 M0 non–small cell lung cancers (NSCLCs),[7,8] lymph node metastases are still found in approximately 20% of clinical T1 N0 M0 lung adenocarcinomas.[9-11] Even for patients with pathologic T1 N0 M0 NSCLCs, tumor involvement of intratumoral vessels or the pleura can also cause local recurrence after limited resection because of the spread of tumor cells into lymphatic vessels outside the primary tumor. To predict which T1 N0 M0 lung adenocarcinomas are curable with limited resection from CT findings, several reports have evaluated the importance of ground-glass opacity (GGO) within tumors, usually indicating bronchioloalveolar carcinoma–like spread because adenocarcinomas with GGO appearance are more frequently N0 stage and have less tumor involvement of intratumoral vessels or pleura than those with a solid appearance.[12,13] The criteria of defining GGO appearance on CT scans are subjective, however, potentially leading to erroneous selection of limited surgical intervention.

In recent years, fluorodeoxyglucose (FDG) positron emission tomography (PET) has been used to evaluate pulmonary nodules and tumor stages. It has been reported that FDG uptake correlates with the proliferative activity of tumors[14,15] and is an independent prognostic factor,[16,17] particularly in lung adenocarcinoma. The prognosis in lung adenocarcinoma is known to depend on not only tumor stage but also tumor involvement of intratumoral vessels or pleura.[9,10,18] To predict lymph node metastases and tumor involvement of intratumoral vessels or pleura in clinical T1 N0 M0 lung adenocarcinomas, we measured FDG uptake to determine any correlation with lymph node metastases, lymphatic and vascular invasion, and pleural involvement.

Materials and Methods

Patients

From December 2001 through October 2003, prospective FDG-PET and CT scans were performed for 223 noncalcified pulmonary nodules. Of these, 93 nodules were malignant tumors less than 3 cm in diameter on CT. Clinical TNM stage was determined by using both CT and PET scanning. Of the 93 malignant nodules, 48 were clinical T1 N0 M0 adenocarcinomas of the lung, and these underwent major lung resection with mediastinal lymph node dissection. We excluded 4 adenocarcinomas less than 1 cm in diameter that were PET negative because the spatial resolution of the current generation of PET scanners is 0.7 to 0.8 cm, making it difficult to image pulmonary nodules of less than 1 cm. As a result, we studied 44 adenocarcinomas that were clinically staged as T1 N0 M0 of sizes from 1 to 3 cm. The medical record of each patient was examined with regard to age, sex, maximum tumor diameter, serum level of carcinoembryonic antigen (CEA; <5 ng/mL vs ≥5 ng/mL), operative procedure, pathologic TNM stage, vascular or lymphatic invasion within tumors (positive vs negative), pleural involvement (p0 vs p1 to p3), and grade of histologic differentiation. To identify tumor involvement of the intratumoral vessels or pleura, we routinely conducted elastica-van Gieson staining. Pleural involvement was classified as p0, p1, p2, or p3; that is, a p0 tumor did not extend beyond the elastic pleural layer, a p1 tumor invaded the visceral pleural elastic layer but did not reach the pleural surface, a p2 tumor included tumor exposure on the pleural surface, and a p3 tumor invaded the parietal pleura or chest wall. The tumor stages were based on the TNM classification of the International Union Against Cancer[19]: p2 tumors were classified as T2; p3 tumors were classified as T3; and tumors with intrapulmonary metastasis within the same lobe were classified as T4. Grades of histologic differentiation were classified as well, moderately, or poorly differentiated.

FDG-PET Scanning

Patients were instructed to fast for at least 4 hours before intravenous administration of fluorine 18–tagged FDG. The dosage of fluorine 18–tagged FDG administered was 125 μCi/kg (4.6 MBq/kg) of body weight for nondiabetic patients and 150 μCi/kg (5.6 MBq/kg) of body weight for diabetic patients. PET imaging was performed approximately 60 minutes after administration of FDG with a POSICAM.HZL mPOWER (Positron Co, Houston, Tex). No-attenuation-corrected emission scans were initially obtained in 2-dimensional, high-sensitivity mode for 4 minutes per bed position and taken from the vertical skull through to the midthighs. Immediately thereafter, a 2-bed-position attenuation-corrected examination was performed, with 6 minutes for the emission sequence and 6 minutes for the transmission sequence at each bed position. The images were usually reconstructed in a 256 × 256 matrix by using ordered subset expectation maximization corresponding to a pixel size of 4 × 4 mm, with section spacing of 2.66 mm.

PET Data Analysis

The FDG-PET data were evaluated semiquantitatively on the basis of the contrast ratio (CR) obtained as follows. The regions of interest (ROIs) were placed in the nodules and contralateral lung. Highest activities in the tumor ROI (T) and in the contralateral normal lung ROI (N) were measured. The CR was calculated by using the formula $(T - N)/(T + N)$ in each nodule as an index of FDG uptake. After correction for radioactive decay, the ROIs were also analyzed by computing the standard uptake value (SUV), which was calculated on the basis of the following equation: Tumor activity concentration/Injected dose/Body weight. The maximum SUV within the selected ROIs was also measured and compared with the results of CR.

Statistical Analysis

All data were analyzed for significance by using the 2-tailed Student t test. All values in the text and tables are given as means ± SD.

GTS

TABLE 1. Tumor involvements and pathologic TNM stage for each CR value

CR of FDG uptake	Total lesions	>T1 N0 M0*	Lymphatic invasion	Vascular invasion	Pleural involvement
0.3	16	0	5	1	1
0.4	19	0	5	1	1
0.5†	22	0	5	1	1
0.6	29	2	9	2	2
0.7	37	4	14	7	6
0.8	39	4	15	8	6
0.9	43	8	19	10	8
1.0	44	8	19	10	8

*Pathologically more advanced stages than T1 N0 M0. Three of the 8 cases were p2; the other 5 were p1.
†Cutoff value of CR.

TABLE 2. PET findings and patients' characteristics, tumor size, and serum level of CEA

	CR of FDG uptake		P
	<0.5 (n = 22)	≥0.5 (n = 22)	value
Age (y, mean ± SD)	63 ± 11	64 ± 13	NS
Male (No.)	14	10	NS
Female (No.)	8	12	
Tumor size (cm, mean ± SD)	1.9 ± 0.6	2.2 ± 0.4	NS
CEA (ng/mL)			.001
<5.0	22	10	
≥5.0	0	12	

NS, Not statistically significant.

Results

The pathologic tumor stage was T1 N0 M0 in 36 patients and more advanced in 8 patients (ie, T1 N1 M0 in 3 patients, T2 N0 M0 in 3 patients, and T4 N0 M0 in 2 patients). Lymphatic or vascular invasion within tumors and pleural involvement was seen in 19, 10, and 8 patients, respectively. Table 1 shows the various CR values with relation to the pathologic tumor stage, lymphatic and vascular invasion, and pleural involvement. Although all adenocarcinomas with a CR of less than 0.5 were pathologically staged as T1 N0 M0, some adenocarcinomas with a CR of 0.5 or greater were more advanced than T1 N0 M0, with more frequent lymphatic and vascular invasion and pleural involvement than the former. Therefore medical records were compared between the 22 adenocarcinomas with a CR of less than 0.5 and the 22 adenocarcinomas with a CR of 0.5 or greater.

The maximum SUVs ranged from 0.5 to 3.1 (mean, 1.1 ± 0.7) in the 22 adenocarcinomas with a CR of less than 0.5 and from 1.9 to 8.5 (mean, 3.9 ± 1.8) in the 22 adenocarcinomas with CRs of 0.5 or greater, with the difference between the 2 groups being significant ($P < .001$). Two (9%) of the 22 adenocarcinomas with CRs of less than 0.5 showed an SUV of 2.5 or greater, however, both of which were pathologically staged as T1 N0 M0 and had no involvements of intratumoral vessels or pleura. Seven (32%) of the 22 adenocarcinomas with CRs of 0.5 or greater had SUVs of less than 2.5, of which 2 had a more advanced tumor stage than T1 N0 M0, 6 had lymphatic invasion, and 1 had vascular invasion.

TABLE 3. Correlation between PET findings and pathologic tumor stage

		CR of FDG uptake	
Pathologic TNM	Total (n = 44)	<0.5 (n = 22)	≥0.5 (n = 22)
T1 N0 M0	36	22*	14*
T1 N1 M0	3	0	3
T2 N0 M0	3	0	3
T4 N0 M0	2	0	2

T2 is classified from pleural involvement grade, p2. T4 is classified from intrapulmonary metastasis.
*Significant difference in the frequency of T1 N0 M0 between the CR <0.5 and CR ≥0.5 groups ($P = .002$).

Table 2 shows the results of PET findings with patients' characteristics, tumor size, and serum level of CEA. None of the adenocarcinomas with CRs of less than 0.5 had increased serum levels of CEA, which was significantly less frequent than the incidence of increased CEA in the 12 (55%) of 22 adenocarcinomas with CRs of 0.5 or greater ($P < .001$). There was no significant difference between the 2 groups in mean age, sex ratio, or tumor size.

Table 3 shows the correlation between PET findings and pathologic tumor stage. All adenocarcinomas (100%) with CRs of less than 0.5 were staged as T1 N0 M0. Adenocarcinomas with CRs of 0.5 or greater were staged as T1 N0 M0 in 14 (64%) patients, T1 N1 M0 in 3 patients, T2 N0 M0 caused by p2 (tumor exposure on the pleural surface) in 3 patients, and T4 N0 M0 caused by intrapulmonary metastases in 2 patients. Adenocarcinomas with CRs of less than 0.5 were more likely to be pathologic T1 N0 M0 stage than those with CRs of 0.5 or greater ($P = .002$).

Table 4 shows the correlation between PET findings and lymphatic and vascular invasion within tumors and pleural involvement. Lymphatic invasion was seen in 5 (23%) of 22 adenocarcinomas with CRs of less than 0.5, which was significantly less frequent than 14 (64%) of 22 with CRs of 0.5 or greater ($P = .006$). Vascular invasion was seen in 1 (5%) of 22 adenocarcinomas with CRs of less than 0.5, which was significantly less frequent than 9 (41%) of 22 with CRs of 0.5 or greater ($P = .004$). Pleural involvement was seen in 1 (5%) of 22 adenocarcinomas with CRs of less than 0.5, which was significantly less frequent than 7 (32%) of 22 with CRs of 0.5 or greater ($P = .02$).

Table 5 shows the correlation between PET findings and the histologic degree of differentiation. In the adenocarcinomas with CRs of less than 0.5, well-differentiated and

TABLE 4. Correlation between PET findings and tumor involvement into intratumoral vessels or pleura

Tumor involvement	CR of FDG uptake <0.5 (n = 22)	CR of FDG uptake ≥0.5 (n = 22)	P value
Lymphatic invasion			.006
Yes	5	14	
No	17	8	
Vascular invasion			.004
Yes	1	9	
No	21	13	
Pleural involvement			.02
p0	21	15	
p1-p2	1	7	

TABLE 5. Correlation between PET findings and grade of histologic differentiation of adenocarcinomas

Grade of differentiation	Total (n = 44)	CR of FDG uptake <0.5 (n = 22)	CR of FDG uptake ≥0.5 (n = 22)
Well differentiated	23	19*	4*
Moderately differentiated	17	3	14
Poorly differentiated	4	0	4

There was significant difference in frequency of well-differentiated adenocarcinomas between the CR <0.5 and CR ≥0.5 groups ($P < .001$).

TABLE 6. Correlation between PET findings and tumor stages, tumor involvement of intratumoral vessels, and tumor involvement of pleura in well-differentiated adenocarcinomas

Tumor stage and invasiveness	CR of FDG uptake >0.5 (n = 19)	CR of FDG uptake ≥0.5 (n = 4)	P value
TNM stage			<.01
T1 N0 M0	19	2	
>T1 N0 M0	0	2	
Lymphatic invasion			<.001
Yes	3	4	
No	16	0	
Vascular invasion			.02
Yes	1	2	
No	18	2	
Pleural involvement			<.01
p0	19	2	
p1-p2	0	2	

moderately differentiated adenocarcinomas were seen in 19 and 3 patients, respectively. In the adenocarcinomas with CRs of 0.5 or greater, well-differentiated, moderately differentiated, and poorly differentiated adenocarcinomas were seen in 4, 14, and 4 patients, respectively. Adenocarcinomas with CRs of less than 0.5 were more commonly well differentiated than those with CRs of 0.5 or greater ($P < .001$).

Table 6 shows the PET findings in well-differentiated adenocarcinomas with relation to the tumor stages and tumor involvements. Of the 4 well-differentiated adenocarcinomas with CRs of 0.5 or greater, each one (25%) was a pathologic T1 N1 M0 and T4 N0 M0 carcinoma, respectively; 4 (100%) had lymphatic invasion; 2 (50%) had vascular invasion; and 2 (50%) had pleural involvement. The well-differentiated adenocarcinomas with CRs of 0.5 or greater had advanced tumor stages, lymphatic and vascular invasion, and pleural involvement more frequently than those with CRs of less than 0.5 ($P < .01$, $P < .001$, $P = .02$, and $P < .01$, respectively).

Discussion

Although a criterion for diagnosing pulmonary malignancy with FDG-PET has frequently used an SUV with a cutoff value of 2.5,[20] some authors used visual evaluation, such as comparison of FDG uptake between nodules and mediastinal uptake.[21] The present study evaluated FDG uptake with CR instead of SUV for the following reasons: (1)hyperglycemia in diabetic patients decreases both the blood clearance of FDG and the accumulation of FDG in tumor tissue, and (2) SUV could be different between fat and thin patients because it is measured by using a body weight. Actually, the mean SUV of malignant pulmonary nodules has been reported to be various, ranging from 5.5 to 10.1.[22-25] In breast cancer, Wahl and coworkers[26] have demonstrated that a CR between tumor and contralateral normal breast is a reliable indicator for diagnosing malignancy. We accordingly used CR in the present study and determined that the cutoff value to differentiate between aggressive and nonaggressive adenocarcinomas was 0.5, with which we could differentiate the degree of tumor aggressiveness more accurately than with SUV.

The important points of the present study are as follows. Compared with adenocarcinomas with CRs of 0.5 or greater, those with CRs of less than 0.5 (1) did not show an increased serum level of CEA, (2) did not have lymph node metastases, (3) had less tumor involvement of vessels or pleura, and (4) were more frequently well-differentiated adenocarcinomas. The serum level of CEA in lung adenocarcinomas has been reported to be higher in N1 or N2 disease than in N0 disease.[27] FDG uptake in lung adenocarcinomas is known to often be negative in well-differentiated adenocarcinomas.[28] It has been also reported that well-differentiated adenocarcinomas are more commonly N0 stage and have less tumor involvement of vessels or pleura, than moderately or poorly differentiated lesions.[9,12,13,18] Our results agree with those of these earlier studies. There were, however, 4 well-differentiated adenocarcinomas with CRs of 0.5 or greater that had more tumor aggressiveness than the 19 well-differentiated lesions with CRs of less than 0.5. We therefore consider that an FDG

GTS

uptake on PET can predict lymph node metastases and tumor invasiveness more accurately than the grade of histologic differentiation in clinical T1 N0 M0 adenocarcinomas.

Although limited resection could be a reasonable approach for T1 N0 M0 lung cancers, it has been reported that lymph node metastases are found in about 20% of clinical T1 N0 M0 adenocarcinomas.[9-11] In 1995, the Lung Cancer Study Group reported the results of a randomized control trial comparing limited resection and lobectomy for clinical T1 N0 M0 NSCLCs.[29] This trial demonstrated the inferiority of limited resection in terms of local relapse and prognosis because some patients actually had pathologic N1 or N2 disease. This is also because tumor involvement of intratumoral vessels or the pleura can cause local recurrence after limited resection, even for pathologic N0 disease, because of the spread of tumor cells into lymphatic vessels outside the primary tumor.[30] The present study showed that clinical T1 N0 M0 adenocarcinomas with CRs of less than 0.5 usually did not metastasize to the lymph nodes and seldom invaded the intratumoral vessels or pleura. This type of lung adenocarcinoma can be cured by means of limited surgical resection, such as segmentectomy or wedge resection. Although it has been reported that NSCLCs of less than 2 cm in size can be cured by means of segmentectomy with mediastinal lymph node dissection (ie, extended segmentectomy),[7] the indication of the extended segmentectomy could be expanded for adenocarcinomas with CRs of less than 0.5 that are less than 3 cm in size.

Mediastinal lymph node dissection is a useful procedure to secure complete local control of an NSCLC, with a subsequent improvement in both survival and nodal staging.[11] However, to minimize the damage caused by mediastinal node dissection in the patients with clinical stage I NSCLC, several authors reduced the dissection of some mediastinal lymph nodal stations with respect to the location of the primary tumor (ie, that the inferior and superior mediastinal lymph node stations could be reduced in the upper lobectomy and lower lobectomy, respectively).[31,32] To expand the possibility of reduction of mediastinal lymph node dissection, a successful intraoperative sentinel lymph node biopsy has been reported.[33,34] The present study showed that lymph node dissection could be reduced for clinical T1 N0 M0 adenocarcinomas with CRs of less than 0.5, without using the sentinel lymph node biopsy.

Although FDG-PET is well known to be useful for tumor staging in lung cancer, we believe that it can also predict lymph node metastases and tumor invasiveness in clinical T1 N0 M0 lung adenocarcinomas. Limited lung resection could be indicated, lymph node dissection or mediastinoscopy could be reduced, or both in this type of adenocarcinoma.

References

1. Kaneko M, Eguchi K, Ohmatsu H, et al. Peripheral lung cancer: screening and detection with low-dose spiral CT versus radiography. *Radiology*. 1996;201:798-802.
2. Yankelevitz DF, Gupta R, Zhao B, Henschke CI. Small pulmonary nodules: evaluation with repeat CT-preliminary experience. *Radiology*. 1999;212:561-6.
3. Henschke CI, Yankelevitz DF. CT screening for lung cancer. *Radiol Clin North Am*. 2000;38:487-95.
4. Nomori H, Horio H, Fuyuno G, Kobayashi R, Morinaga S, Suemasu K. Lung adenocarcinomas diagnosed by open or thoracoscopic vs. bronchoscopic biopsy. *Chest*. 1998;114:40-4.
5. Nomori H, Horio H. Colored collagen is a long-lasting point marker for small pulmonary nodules in thoracoscopic operations. *Ann Thorac Surg*. 1996;61:1070-3.
6. Nomori H, Horio H, Naruke T, Suemasu K. Fluoroscopy-assisted thoracoscopic resection of lung nodules marked with lipiodol. *Ann Thorac Surg*. 2002;74:170-3.
7. Yoshikawa K, Tsubota N, Kodama K, Ayabe H, Taki T, Mori T. Prospective study of extended segmentectomy for small lung tumors. *Ann Thorac Surg*. 2002;73:1055-9.
8. Kodama K, Doi O, Higashiyama M, Yokouchi H. Intentional limited resection for selected patients with T1 N0 M0 non-small cell lung cancer. *J Thorac Cardiovasc Surg*. 1997;114:347-53.
9. Suzuki K, Nagai K, Yoshida J, Nishimura M, Nishizaki Y. Predictors of lymph node and intrapulmonary metastasis in clinical stage IA non-small cell lung carcinoma. *Ann Thorac Surg*. 2001;72:352-6.
10. Asamura H, Nakayama H, Kondo H, Tsuchiya R, Shimosato Y, Naruke T. Lymph node involvement, recurrence, and prognosis in resected small, peripheral, non-small cell lung carcinomas: are these carcinomas candidates for video-assisted lobectomy? *J Thorac Cardiovasc Surg*. 1996;111:1125-34.
11. Naruke T, Goya T, Tsuchiya R, Suemasu K. The importance of surgery of non-small cell carcinoma of lung with mediastinal lymph node metastasis. *Ann Thorac Surg*. 1998;46:603-10.
12. Suzuki K, Asamura H, Kusumoto M, Kondo H, Tsuchiya R. Early peripheral lung cancer: prognostic significance of ground glass opacity on thin-section computed tomographic scan. *Ann Thorac Surg*. 2002; 74:1635-9.
13. Matsuguma H, Yokoi K, Anraku M, et al. Proportion of ground-glass opacity on high-resolution computed tomography in clinical T1 N0 M0 adenocarcinoma of the lung: a predictor of lymph node metastasis. *J Thorac Cardiovasc Surg*. 2002;124:278-84.
14. Higashi K, Ueda Y, Yagishita M, et al. FEG PET measurement of the proliferative potential of non-small cell lung cancer. *J Nucl Med*. 2000;41:85-92.
15. Vesselle H, Schmidt RA, Pugsley JM, et al. Lung cancer proliferation correlates with [F-18]fluorodeoxyglucose uptake by positron emission tomography. *Clin Cancer Res*. 2000;6:3837-44.
16. Ahuja V, Coleman RE, Herndon J, Patz EF. The prognostic significance of fluorodeoxyglucose positron emission tomography imaging for patients with non-small cell lung carcinoma. *Cancer*. 1998;83:918-24.
17. Vansteenkiste JF, Stroobants SG, Dupont PJ, et al. Prognostic importance of the standardized uptake value on ^{18}F-fluoro-2-deoxy-glucose-positron emission tomography in non-small cell lung cancer: an analysis of 125 cases. *J Clin Oncol*. 1999;17:3201-6.
18. Noguchi M, Morikawa A, Kawasaki M, et al. Small adenocarcinoma of the lung. Histologic characteristics and prognosis. *Cancer*. 1995; 75:2844-52.
19. Sobin LH, Wittekind Ch, editors. UICC: TNM classification of malignant tumours. 6th ed. New York: John Wiley & Sons; 2002. p. 99-103.
20. Coleman RE. PET in lung cancer. *J Nucl Med*. 1999;40:814-20.
21. Marom EM, Sarvis S, Herndon JE, et al. T1 lung cancers: sensitivity of diagnosis with fluorodeoxyglucose PET. *Radiology*. 2002;223: 453-9.
22. Dewan NA, Gupta NC, Redepenning LS, et al. Diagnostic efficacy of PET-FDG imaging in solitary pulmonary nodules. *Chest*. 1993;104: 997-1002.
23. Gupta NC, Maloof J, Gunel E. Probability of malignancy in solitary

pulmonary nodules using fluorine-18-FDG and PET. *J Nucl Med.* 1996;37:943-8.
24. Imdahl A, Jenkner S, Brink I, et al. Validation of FDG positron emission tomography for differentiation of unknown pulmonary lesions. *Eur J Cardiothorac Surg.* 2001;20:324-9.
25. Lowe VJ, Fletcher JW, Gobar L, et al. Prospective investigation of positron emission tomography in lung nodules. *J Clin Oncol.* 1998; 16:1075-84.
26. Wahl RL, Cody RL, Hutchins GD, et al. Primary and metastatic breast carcinoma: initial clinical evaluation with PET with the radiolabeled glucose analogue 2-[F-18]-fluoro-2-deoxy-D-glucose. *Radiology.* 1991;179:765-70.
27. Takamochi K, Nagai K, Yoshida J, et al. Pathologic N0 status in pulmonary adenocarcinoma is predictable by combining serum carcinoembryonic antigen level and computed tomographic findings. *J Thorac Cardiovasc Surg.* 2001;122:325-30.
28. Higashi K, Ueda Y, Seki H. F-18 FDG PET imaging is negative in bronchiolo-alveolar lung carcinoma. *J Nucl Med.* 1998;39:1016-20.
29. Ginsberg RJ, Rubinstein LV. Randomized trial of lobectomy versus limited resection for T1N0 non-small cell lung cancer. Lung Cancer Study Group. *Ann Thorac Surg.* 1995;60:615-22.
30. Ichinose Y, Yano T, Yokoyama H, Inoue T, Asoh H, Katsuda Y. The correlation between tumor size and lymphatic vessel invasion in resected peripheral stage I non-small cell lung cancer. A potential risk of limited resection. *J Thorac Cardiovasc Surg.* 1994;108:684-6.
31. Naruke T, Tsuchiya R, Kondo H, Nakayama H, Asamura H. Lymph node sampling in lung cancer: how should it be done? *Eur J Cardiothorac Surg.* 1999;16(suppl):S17-24.
32. Asamura H, Nakayama H, Kondo H, Tsuchiya R, Naruke T. Lobe-specific extent of systemic lymph node dissection for non-small cell lung carcinomas according to a retrospective study of metastases and prognosis. *J Thorac Cardiovasc Surg.* 1999;117:1102-11.
33. Liptay MJ, Masters GA, Winchester DJ, et al. Intraoperative radioisotope sentinel lymph node mapping in non-small cell lung cancer. *Ann Thorac Surg.* 2000;70:384-90.
34. Nomori H, Horio H, Naruke T, Orikasa H, Yamazaki K, Suemasu K. Use of technetium-99m tin colloid for sentinel lymph node identification in non-small cell lung cancer. *J Thorac Cardiovasc Surg.* 2002; 124:486-92.

GTS

Progression of Focal Pure Ground-Glass Opacity Detected by Low-Dose Helical Computed Tomography Screening for Lung Cancer

Ryutaro Kakinuma, MD, Hironobu Ohmatsu, MD, Masahiro Kaneko, MD, Masahiko Kusumoto, MD, Junji Yoshida, MD, Kanji Nagai, MD, Yutaka Nishiwaki, MD, Toshiaki Kobayashi, MD, Ryosuke Tsuchiya, MD, Hiroyuki Nishiyama, MD, Eisuke Matsui, MD, Kenji Eguchi, MD, and Noriyuki Moriyama, MD

Objective: To clarify the progression of focal pure ground-glass opacity (pGGO) detected by low-dose helical computed tomography (CT) screening for lung cancer.

Methods: A total of 15,938 low-dose helical CT examinations were performed in 2052 participants in the screening project, and 1566 of them were judged to have yielded abnormal findings requiring further examination. Patients with peripheral nodules exhibiting pGGO at the time of the first thin-section CT examination and confirmed histologically by thin-section CT after follow-up of more than 6 months were enrolled in the current study. Progression was classified based on the follow-up thin-section CT findings.

Results: The progression of the 8 cases was classified into 3 types: increasing size (n = 5: bronchioloalveolar carcinoma [BAC]), decreasing size and the appearance of a solid component (n = 2: BAC, n = 1; adenocarcinoma with mixed subtype [Ad], n = 1), and stable size and increasing density (n = 1: BAC). In addition, the decreasing size group was further divided into 2 subtypes: a rapid-decreasing type (Ad: n = 1) and a slow-decreasing type (BAC: n = 1). The mean period between the first thin-section CT and surgery was 18 months (range: 7–38 months). All but one of the follow-up cases of lung cancer were noninvasive whereas the remaining GGO with a solid component was minimally invasive.

Conclusions: The pGGOs of lung cancer nodules do not only increase in size or density, but may also decrease rapidly or slowly with the appearance of solid components. Close follow-up until the appearance of a solid component may be a valid option for the management of pGGO.

Key Words: ground-glass opacity, low-dose helical computed tomography screening, lung cancer

(*J Comput Assist Tomogr* 2004;28:17–23)

Focal pure ground-glass opacities (pGGOs), or nodules of the lungs, has become a major concern as low-dose helical computed tomography (CT) screening for lung cancer becomes more widely available, not only in the field of diagnostic imaging,[1–5] but also in the field of limited surgery.[6–10] GGO is a finding on thin-section CT images of the lung which has been described as a hazy, increased attenuation of the lung tissue with preservation of the bronchial and vascular margins. GGO is usually a nonspecific finding that is found in many types of pulmonary disease.[11] However, some investigators have recently reported that most localized pGGOs or focal GGOs are malignant.[1,2,5] Although a few reports have described the evolution of lung cancer using conventional chest CT,[12–14] thin-section CT[15–17] and low-dose screening CT,[18,19] the natural history of peripheral lung cancers that exhibit as pGGO on thin-section CT images detected using low-dose helical CT screening is still unclear.

The purpose of this retrospective study was to clarify the progression of pGGOs, which were not visible on chest radiographs, detected by low-dose helical CT screening examinations performed every 6 months. We evaluated the progression of pGGOs based on the thin-section CT findings obtained during the follow-up after the first thin-section CT.

PATIENTS AND METHODS

Subjects

Between September 1993 and January 2003, low-dose helical CT screening was conducted semiannually in Tokyo by

From the Division of Thoracic Oncology (Drs Kakinuma, Ohmatsu, Yoshida, Nagai, and Nishiwaki), National Cancer Center Hospital East, Tsukiji, Chiba Japan; the Divisions of Endoscopy (Drs Kaneko and Kobayashi), Diagnostic Radiology (Drs Kusumoto and Moriyama), and Thoracic Surgery (Dr Tsuchiya), National Cancer Center Hospital; the Division of Thoracic Surgery (Dr Nishiyama), Social Health Insurance Medical Center, Okubo, Japan; (Dr Matsui); the Anti–Lung Cancer Association, Ichigaya, Japan; and the Division of Internal Medicine (Dr Eguchi), School of Medicine, Tokai University, Isehara, Japan.

This study was supported in part by a Grant-in-Aid for Cancer Research (13-8) from the Ministry of Health, Labor, and Welfare of Japan and by a Grant-in-Aid from the Second-Term Comprehensive 10-Year Strategy for Cancer Control.

Reprints: Ryutaro Kakinuma, MD, National Cancer Center Hospital East, 6-5-1 Kashiwa-no-ha, Kashiwa, Chiba 277-8577, Japan (e-mail: rkaki@east.ncc.go.jp).

the Anti–Lung Cancer Association (ALCA), a for-profit organization for lung cancer screening.[20,21] Each screening consisted of a low-dose helical CT examination, chest radiography, and cytologic sputum studies. During this period, a total of 15,938 low-dose helical CT examinations were performed in 2052 ALCA members. Among the low-dose helical CT examinations, a total of 1566 CT examinations were judged as having abnormal findings requiring further examination. Sixty-seven cases of lung cancer (peripheral-type lung cancer, 61; hilar-type lung cancer, 6) were detected during the ALCA lung cancer screening project. Out of these 67 cases, 51 cases (76%) were pathologic stage IA. The treatments used in the 67 cases were as follows: surgery (n = 55), radiotherapy (n = 5), radiotherapy and chemotherapy (n = 2), chemotherapy (n = 4), and photodynamic therapy (n = 1). Among the patients with peripheral nodules detected by the low-dose helical CT examinations performed every 6 months, the patients with histologically diagnosed nodules exhibiting pGGO larger than 5 mm in diameter at the time of the first thin-section CT and followed-up by thin-section CT for more than 6 months were enrolled in the current study.

CT Scanning Conditions

A TCT900S Superhelix CT scanner (Toshiba Medical Inc., Tokyo, Japan) was used for all of the examinations. Low-dose helical CT screening was performed under the following conditions: 120 kV, 50 mA, beam width of 10 mm, 1 rotation of the x-ray tube per second, and a table speed of 20 mm per second (pitch 2:1). Reconstruction was performed at intervals of 10 mm. The CT images were displayed on a monitor with a window width of 2000 HU and a window level of −700 HU. If newly developed nodules were identified, thin-section CT examinations were performed under the following conditions: 120 kV, 250 mA, beam width of 2 mm, 1 rotation of the x-ray tube per second, and a table speed of 2 mm per second (pitch 1:1). Reconstruction was performed at intervals of 2 mm using a thin-section CT algorithm.

Evaluation of pGGO Progression Patterns

The progression patterns were classified based on changes in the size and density of the pGGOs on the thin-section CT images. The study period was divided into 2 phases: the unidentified phase (ie, the period prior to the first thin-section CT scan) and the follow-up phase (ie, the period after the first thin-section CT scan). CT images of the pGGOs in the unidentified phase were reviewed independently by 4 physicians (R.K., M.K., H.O., K.E.), who are diagnostic experts in chest radiology, and by 1 radiologist (M.K.). CT findings were adopted as positive findings if 3 of more of the doctors agreed. After the independent reviews, we decided by consensus as to how many pGGOs were newly developed or had arisen from inconspicuous nodules during the helical CT screening period. In the follow-up phase, the size of the pGGOs was measured with a pair of calipers on the thin-section CT images obtained during the initial scan and the final scan by consensus of 2 diagnostic experts (R.K., M.K.) to assess doubling time. The size of the lesion was evaluated using measurements that passed through the center of the lesion. Size was defined as the average of the length and width of the lesion. Doubling times were calculated using the Schwartz equation.[22] The density of faint opacities was evaluated visually on the thin-section CT images obtained during the follow-up phase. pGGO was defined as a homogeneous GGO, and mixed GGO was defined as a GGO with a solid component.

Pathologic Classification of Adenocarcinomas

The histologic findings of the adenocarcinomas were classified according to the criteria of the World Health Organization (WHO)[23] and the criteria of Noguchi et al.[24] The classification system for replacement growth patterns developed by Noguchi et al is as follows: type A (localized bronchioloalveolar carcinoma; LBAC), type B (LBAC with foci of collapsed alveolar structure), and type C (LBAC with foci of active fibroblastic proliferation).

RESULTS

Patient Characteristics

Eight patients with pGGOs (6 men and 2 women) were enrolled in the current study (Table 1). The patients ranged in age from 49 to 69 years (mean, 64 years). With regard to smoking history, 3 patients were nonsmokers, 4 were ex-smokers, and 1 was a current smoker. Four of these 8 pGGO patients were not apparent during the initial screening and became apparent during the screening period, and 3 of the other 4 pGGO patients with inconspicuous opacities visible in retrospect during the initial screening became apparent later. In 1 other case, a conspicuous opacity and multiple old tuberculosis lesions were observed during the initial CT screening. The locations of the pGGOs were as follows: right upper lobe (n = 4), right lower lobe (n = 1), left upper lobe (n = 1), and left lower lobe (n = 2).

Clinical Course

The period between the first visible nodule of a pGGO on a thin-section CT image and the first visible opacity on a helical CT screening image when viewed retrospectively ranged from 13 to 46 months (mean, 22 months) (Table 1). The period between the first thin-section CT examination and the surgery ranged from 7 to 39 months (mean, 19 months). The interval between the last thin-section CT examination and surgery ranged from 1 to 98 days (mean, 32 days).

Histology of GGOs

Seven patients had bronchioloalveolar carcinoma (BAC), defined as noninvasive by the WHO classification in 1999, and 1 had an adenocarcinoma with mixed subtypes (Table 1). Based on Noguchi's classification for small adeno-

TABLE 1. Clinical Characteristics and Histology of Ground-Glass Opacities

Case No.	Sex	Age at Detection (Years)	Smoking Index	Development	Lobe	Period Between: First Visible and the First TS-CT (Months)*	Period Between: The First TS-CT and Surgery (Months)*	Period Between: The Last TS-CT and Surgery (Days)	Histology: WHO Classification	Histology: Noguchi Type
1	M	69	1300	New	RU	41	13	1	Ad	C
2	M	69	800 (ex)	New	RU	13	39	36	BAC	B
3	F	66	Non	New	LL	13	14	33	BAC	A
4	M	66	450 (ex)	New	LU	18	26	98	BAC	A
5	F	65	Non	ic	LL	46	28	13	BAC	B
6	M	69	800 (ex)	ic	RU	21	12	13	BAC	A
7	M	49	515 (ex)	ic	RU	14	10	6	BAC	A
8	M	63	Non	c	RL	13	7	57	BAC	B

Non, nonsmoker; ex, ex-smoker; ic, inconspicuous; c, conspicuous; RU, right upper lobe; LU, left upper lobe; LL, left lower-lobe; TS-CT, thin-section CT; BAC, bronchioloalveolar carcinoma; Ad, adenocarcinoma.
*Number of months was rounded.

carcinomas, the pGGOs consisted of 4 cases of type A and 2 cases of type B while the mixed GGOs consisted of 1 case of type B and 1 case of type C (Tables 1, 2). All the lung cancers were diagnosed at pathologic stage IA.

Progression of pGGOs

The period between the first thin-section CT and the final thin-section CT examinations ranged from 6 to 37 months (mean, 17 months) (Table 2). The opacities ranged in size from 6.5 mm to 17 mm (mean, 10 mm) at the time of the first thin-section CT examination and from 7 mm to 16.5 mm (mean, 10.5 mm) at the time of the final thin-section CT examination.

The progressions of 8 opacities in the follow-up phase were classified into 3 types: increasing in size (Increasing type, n = 5), decreasing in size and the appearance of a solid component (decreasing type, n = 2), and stable in size and increasing in density (density type, n = 1). In addition, the decreasing type was classified into 2 subtypes: a rapid-decreasing type (case 1, Fig. 1; decrease in size at the time of the 6-month follow-up) and a slow-decreasing type (case 2, Fig. 2; decrease after follow-up for more than 1 year). All but 1 of the follow-up cases were noninvasive, and the remaining GGO with a solid component was judged to be minimally invasive adenocarcinoma because the size of the collapse fibrosis was only 2 mm in diameter (Fig. 1F).

TABLE 2. Thin-Section CT Findings, Progression Types, and Doubling Time of Ground-Glass Opacities

Case No.	Follow-Up Phase with Thin-Section CT: GGO Size (mm) First	GGO Size (mm) Final	Final TS-CT of GGO: Density	Solid	Finding	Progression Type	Period of Follow-Up with TS-CT (Months)*	GGO Doubling Time (Days)
1	17	12	Increasing	+	Mixed	Dec	12	−214
2	14	12	Increasing	+	Mixed	Dec	37	−1680
3	6.5	7.5	Stable	−	Pure	Inc	13	617
4	7	10.5	Stable	−	Pure	Inc	22	383
5	7	7	Increasing	−	Pure	Den	27	—
6	8.5	9.5	Stable	−	Pure	Inc	12	669
7	6.5	9	Stable	−	Pure	Inc	10	216
8	13.5	16.5	Stable	−	Pure	Inc	6	198

CT, computed tomography; GGO, ground-glass opacity; TS-CT, thin-section computed tomography; Inc, increasing; Dec, decreasing; Den, density.
*Number of months was rounded.

TABLE 3. Evolution of Solid Components in Ground-Glass Opacities

Case No.	Follow-Up Phase with TS-CT Solid Size (mm): First TS-CT	Months After the First TS-CT: 6	11	23	36	Doubling Time (Days)
1	0*	8				14*
2	0	—	2	3	7.5	130†

TS-CT, thin-section computed tomography.

*Doubling time of solid component in case 1 was calculated on the assumption that the first size was 0.5 mm.

†Doubling time of solid component in case 2 was calculated based on the sizes between 11 months and 36 months after the first TS-CT.

Doubling Time

The doubling times of the increasing-type opacities ranged from 198 to 669 days (mean ± SD, 417 ± 220 days). The doubling time of the density-type opacity could not be calculated because it did not change in size. For the decreasing-type opacities, the doubling times were calculated based on the sizes of the pGGOs and the solid components, individually. In case 1, the doubling times of the pGGO and the solid component were −214 and 14 days, respectively. In case 2, the doubling times of the pGGO and the solid component were 1680 and 130 days, respectively.

Correlation of Thin-Section CT Images and Pathologic Findings

The pGGO corresponded to the lepidic growth of cancer cells (Fig. 1E), the thickening of the alveolar wall (Fig. 1E), and the collapse of the alveolar space (Fig. 1E). Solid components corresponded not only to the collapse of the alveolar space and fibrosis (Fig. 1F and Fig. 2G), but also to a severe narrowing of the alveolar space (Fig. 1F). With the development of a solid component in case 2, the distance between the surrounding pulmonary veins and the bronchus gradually narrowed (Figs. 2C–F). The same finding was observed in case 1 (Figs. 1C, D).

DISCUSSION

To our knowledge, this study is the first report to describe the progression of pGGOs in minute lung cancers that appeared as new pGGOs during the screening process or arose from inconspicuous minute nodules on low-dose helical CT screening images obtained at 6-month intervals. In addition, the progressions of the pGGOs on the thin-section CT images were classified into 3 types for the first time. Although a few papers have described the natural history of GGOs in pulmonary adenocarcinoma,[4,7,12,15–17] only 1 researcher[15] reported 2 GGOs that decreased in size, but the size reduction occurred in mixed GGOs, not in pGGOs. The rapid decreasing of a pGGO and the appearance of a solid component has not previously been reported.

Radiologic-pathologic correlations revealed that pGGOs on thin-section CT images mainly represent the lepidic growth of adenocarcinomas.[1,3,4,12,15–17] Solid components in the mixed GGOs were caused by the collapse of alveolar spaces or regions of fibrosis[12] and by a severe narrowing of the alveolar space (case 1). The narrowing of the distance between the surrounding pulmonary vessels and the bronchus was caused not only by the collapse of the alveolar space (cases 1 and 2), but also by the development of fibrosis (case 1) in the pGGO lesions. This finding has been termed "vessel convergence."[12,15,17] Based on our observations of the progression from a pure GGO to a mixed GGO in cases 1 and 2, our results also support the stepwise progression of replacement-type adenocarcinoma.[12,15,17]

Although 1 researcher raised serious questions about the concept of 2-year stability implying benignity,[25] pulmonary nodules are generally considered to be benign if they remain the same size or decrease in size over a 2-year observation period.[26,27] However, our results show that stability or reduction in size over a 2-year period does not necessarily indicate benignity. In the case of a pGGO that decreases in size, can the Schwartz equation be applied to a change from a pGGO to a mixed GGO if the area of the GGO decreases? Usually, the Schwartz equation is based on the assumption that constant exponential tumor growth is the basic pattern of neoplastic proliferation.[22] The doubling time for mixed GGOs has been reported to be 457 ± 260 days.[28] However, progression to a mixed GGO in a case where the pGGO decreases in size and a solid component simultaneously appears has not previously been reported. Moreover, the calculation of doubling times for each component in a mixed GGO has never, to the best of our knowledge, been performed prior to the current study. The doubling time for the solid component in case 1 was calculated based on the assumption that the initial size of the solid component was 0.5 mm, this because the thin-section CT images were taken not only by the single-slice CT scanner described above, but by a multislice CT scanner with the imaging parameters set at 0.5 mm × 4 rows and image reconstruction performed at 1-mm intervals.

Whether pGGOs should be resected or followed up is controversial. Definite evidence of the natural history of pGGOs does not exist at present. However, based on the indirect corroboration described below, we suggest that close follow-up until the appearance of a solid component may be a valid option for the management of pGGO. First, most pGGOs are either atypical adenomatous hyperplasia (preinvasive lesions according to the 1999 WHO criteria), BAC (a noninvasive lesion), or minimally invasive adenocarcinoma.[1,8,29] Second, 1 researcher[7] has previously reported information concerning

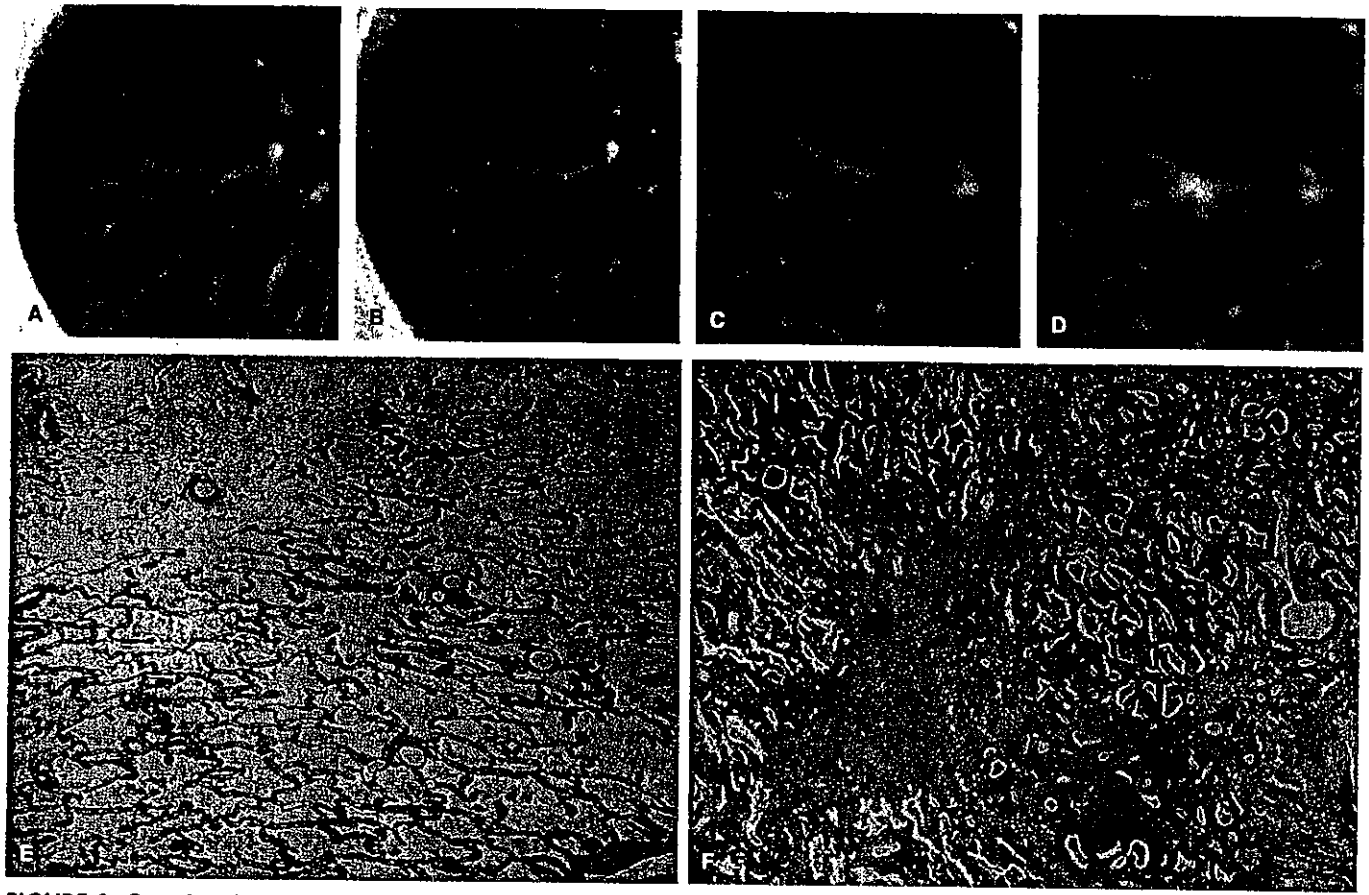

FIGURE 1. Case 1: Adenocarcinoma in a 69-year-old man. A, A faint localized increase in density was identified in segment 1 of the right upper lobe of the lung on a CT screening image obtained in December 2001. B, In retrospect, the opacity was also present on a CT screening image obtained in June 1998. C, Thin-section CT image obtained in December 2001 showing a pGGO in segment 1 of the right upper lobe of the lung. D, Thin-section CT image obtained in June 2002 shows a decrease in the size of the pGGO and the appearance of a solid component. E, Medium-magnification image of the pathologic specimen (H&E staining, ×40). Thickening of the alveolar walls as a result of the tumor cells is visible. F, Medium-magnification image of the pathologic specimen (H&E staining, ×40). Severe narrowing of the alveolar space from the thickening of the alveolar walls and an area of collapse-fibrosis with active fibroblastic proliferation are visible. A right upper lobectomy was performed in January 2003. The lesion was diagnosed as an adenocarcinoma, 17 mm in diameter (Noguchi type C). The size of collapse- fibrosis was 2 mm in diameter.

the natural history of pGGOs after conducting a long-term follow-up study lasting more than 2 years. Five of the 19 cases of pGGOs were diagnosed as lung cancers, that is, 5 BACs (1 case had 2 BACs) and 1 adenocarcinoma, after a mean follow-up of 61 months. Although the patient with adenocarcinoma was followed up for 124 months, personal communication with the author revealed that his lung cancer was of pathologic stage IA and that the size of the central fibrosis of the adenocarcinoma was less than 3 mm in diameter. We have also experienced 2 other pGGOs that developed into mixed GGOs after a 1-year and a 3-year follow-up period, respectively (unpublished data). These lesions were diagnosed as pathologic stage IA adenocarcinomas, and the size of the central fibrosis was 1.5 mm and 2 mm in diameter, respectively. Regarding the relationship between central fibrosis and prognosis, our research team[30] previously reported that 21 out of 100 patients with a lung adenocarcinoma that was 3 cm or less in diameter and which had a central fibrosis of 5 mm or less in diameter had a 5-year survival rate of 100%. Therefore, the adenocarcinoma follow-up cases described above and in this study were thought to be minimally invasive, allowing the possibility of a cure. Third, the adenocarcinoma cases with mixed GGOs did not experience any relapses or deaths, even though the solid components of the GGOs became larger but remained less than 50% of the mixed GGO nodule, this from the standpoint of the GGO's length,[31] the vanishing ratio of GGO[10] ("air-containing type"), and the volume of the GGO.[9] Finally, adenocarcinoma pGGOs tend to grow slowly, as the mean doubling time of pGGOs has been reported to be 813 days[28] or 880 days.[12] In addition, one-fourth of the GGOs in 1 study were

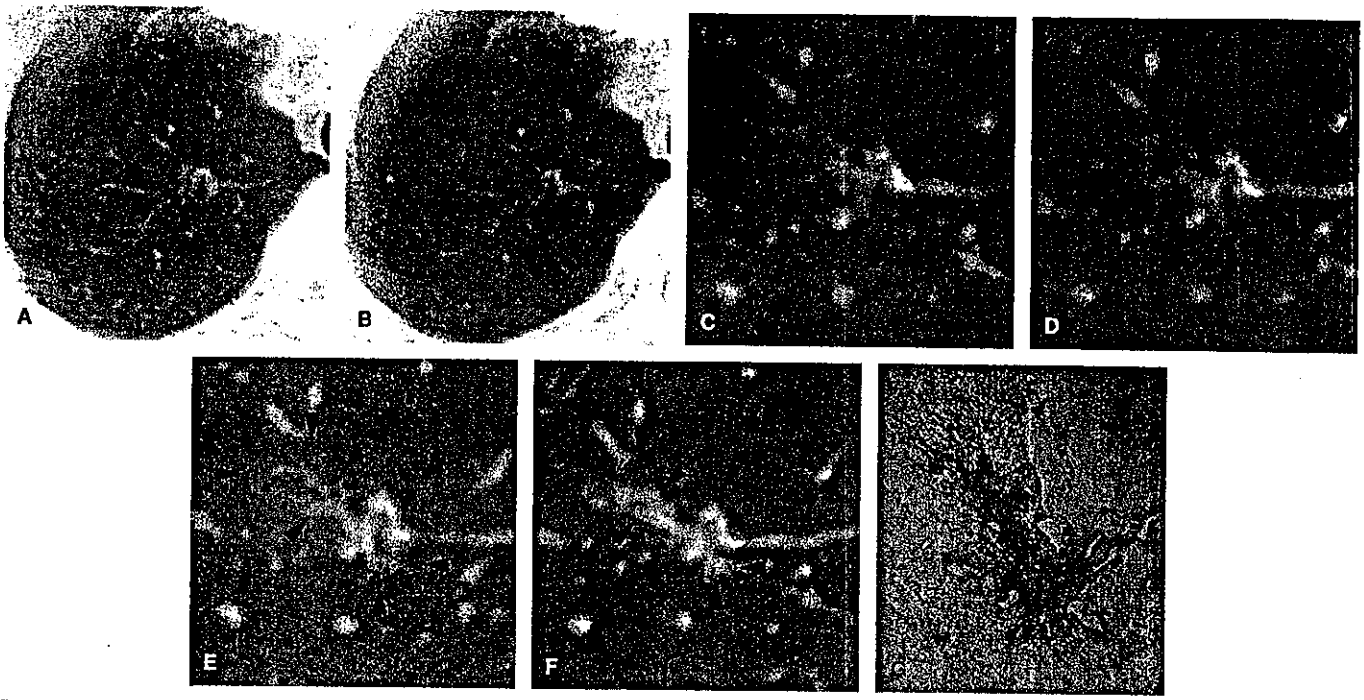

FIGURE 2. Case 2: Bronchioloalveolar carcinoma in a 69-year-old man. A, A faint localized increase in density was identified in segment 1 of the right upper lobe of the lung on a CT screening image obtained in February 1999. B, In retrospect, the opacity was also visible on a CT screening image obtained in February 1998. C, Thin-section CT revealed a pGGO in segment 1 of the right upper lobe of the lung in March 1999. D, Thin-section CT image obtained in February 2000 showing a pGGO with a small solid component. E, Thin-section CT image obtained in February 2001 showing a decrease in the size of the pGGO and a slight increase in the size of the solid component. F, Thin-section CT image obtained in February 2002 showing a larger decrease in the size of the pGGO and an increase in the size of the solid component. G, Low-magnification image of the pathologic specimen (H&E staining, ×5). The foci of alveolar collapse (asterisks) are shown. A right upper lobectomy was performed in May 2002. The lesion was diagnosed as a bronchioloalveolar carcinoma, 15 mm in diameter (Noguchi type B).

stable after a mean follow-up period of 16 months,[17] whereas half of the pGGOs in another study showed no change in size after a median follow-up period of 32 months.[7] Therefore, the classification of some pGGOs may be affected by an overdiagnosis bias.

This study has some limitations. First, the period of pGGO development was not accurately assessed because only thick-sectioned screening CT images were available for the unidentified phase. Therefore, the partial volume effect affected the detectability of small faint opacities on screening CT images. Multislice CT imaging using a narrow collimation and thinner reconstruction images may reveal the natural history of pGGOs more precisely. Second, measurements made with a pair of calipers to calculate doubling times may lead to measurement errors. Although technical advances have been reported,[32,33] we did not have any commercial software for volume measurements. Third, our study cohort was very small. At the start of the helical CT screening project, surgery without follow-up tended to be recommended in cases with pGGO. After knowledge of pGGOs had accumulated (ie, that most pGGOs consisted of preinvasive, noninvasive, or minimally invasive lesions), our treatment procedure changed.[8] Now, resection is only 1 option, not the only option, as in the past. Because of this, resection data cannot always be obtained, and the number of cases was small as a result.

In conclusion, the natural history of pGGOs detected by helical CT screening for lung cancer was partially revealed. A classification for pGGO progression was proposed based on thin-section CT images obtained during the follow-up phase. The pGGOs of lung cancer nodules do not only increase in size or density, but may also decrease rapidly or slowly with the appearance of solid components. Close follow-up until the appearance of a solid component may be a valid option for the management of pGGO.

ACKNOWLEDGMENTS

The authors thank Fumio Shishido, MD, PhD (Department of Radiology, School of Medicine, Fukushima Medical University) for his encouragement. We also wish to thank the pathologists who assisted in this study: Yoshihiro Matsuno, MD (National Cancer Center Research Institute), Tomoyuki Yokose, MD, and Genichiro Ishii, MD (National Cancer Center Research Institute East). We also thank the physicians, the

technical staff, and the administrative staff of the Anti–Lung Cancer Association in Tokyo.

REFERENCES

1. Nakajima R, Yokose T, Kakinuma R, et al. Localized pure ground-glass opacity on high-resolution CT: histologic characteristics. *J Comput Assist Tomogr*. 2002;26:323–329.
2. Nakata M, Saeki H, Takata I, et al. Focal ground-glass opacity detected by low-dose helical CT. *Chest*. 2002;121:1464–1467.
3. Kuriyama K, Seto M, Kasugai T, et al. Ground-glass opacity on thin-section CT: value in differentiating subtypes of adenocarcinoma of the lung. *AJR Am J Roentgenol*. 1999;173:465–469.
4. Yang ZG, Sone S, Takashima S, et al. High-resolution CT analysis of small peripheral lung adenocarcinomas revealed on screening helical CT. *AJR Am J Roentgenol*. 2001;176:1399–1407.
5. Henschke CI, Yankelevitz DF, Mirtcheva R, et al. CT screening for lung cancer: frequency and significance of part-solid and nonsolid nodules. *AJR Am J Roentgenol*. 2002;178:1053–1057.
6. Kodama K, Higashiyama M, Yokouchi H, et al. Prognostic value of ground-glass opacity found in small lung adenocarcinoma on high-resolution CT scanning. *Lung Cancer*. 2001;33:17–25.
7. Kodama K, Higashiyama M, Yokouchi H, et al. Natural history of pure ground-glass opacity after long-term follow-up of more than 2 years. *Ann Thorac Surg*. 2002;73:386–393.
8. Suzuki K, Asamura H, Kusumoto M, et al. "Early" peripheral lung cancer: prognostic significance of ground-glass opacity on thin-section computed tomographic scan. *Ann Thorac Surg*. 2002;74:1635–1639.
9. Matsuguma H, Yokoi K, Anraku M, et al. Proportion of ground-glass opacity on high-resolution computed tomography in clinical T1N0M0 adenocarcinoma of the lung: a predictor of lymph node metastasis. *J Thorac Cardiovasc Surg*. 2002;124:278–284.
10. Kondo T, Yamada K, Noda K, et al. Radiologic-prognostic correlation in patients with small pulmonary adenocarcinomas. *Lung Cancer*. 2002;36:49–57.
11. Austin JM, Muller NL, Friedman PJ, et al. Glossary of terms for CT of the lung: recommendations of the Nomenclature Committee of the Fleischner Society. *Radiology*. 1996;200:327–331.
12. Aoki T, Nakata H, Watanabe H, et al. Evolution of peripheral lung adenocarcinomas: CT findings correlated with histology and tumor doubling time. *AJR Am J Roentgenol*. 2000;174:763–768.
13. White CS, Romney BM, Mason AC, et al. Primary carcinoma of the lung overlooked at CT: analysis of findings in 14 patients. *Radiology*. 1996;199:109–115.
14. Gurney JW. Missed lung cancer at CT: imaging findings in nine patients. *Radiology*. 1996;199:117–122.
15. Koizumi N, Sakai K, Matsuzuki Y, et al. Natural history of cloudy zone of pulmonary adenocarcinoma on HRCT [in Japanese]. *Nippon Igaku Hoshasen Gakkai Zasshi*. 1996;56:715–719.
16. Jang HJ, Lee KS, Kwon OJ, et al. Bronchioloalveolar carcinoma: focal area of ground-glass attenuation at thin-section CT as an early sign. *Radiology*. 1996;199:485–488.
17. Takashima S, Maruyama Y, Hasegawa M, et al. CT findings and progression of small peripheral lung neoplasms having a replacement growth pattern. *AJR Am J Roentgenol*. 2003;180:817–826.
18. Kakinuma R, Ohmatsu H, Kaneko M, et al. Detection failures in spiral CT screening for lung cancer: analysis of CT findings. *Radiology*. 1999;212:61–66.
19. Li F, Sone S, Abe H, et al. Lung cancers missed at low-dose helical CT screening in a general population: comparison of clinical, histopathologic, and imaging findings. *Radiology*. 2002;225:673–683.
20. Kaneko M, Eguchi K, Ohmatsu H, et al. Peripheral lung cancer: screening and detection with low-dose spiral CT versus radiography. *Radiology*. 1996;201:798–802.
21. Sobue T, Moriyama N, Kaneko M, et al. Screening for lung cancer with low-dose helical computed tomography: Anti–Lung Cancer Association project. *J Clin Oncol*. 2002;20:911–920.
22. Schwartz M. A biomathematical approach to clinical tumor growth. *Cancer*. 1961;14:1272–1294.
23. Travis W, Colby T, Corrin B, et al. *Histological Typing of Lung and Pleural Tumors*. Berlin: Springer; 1999.
24. Noguchi M, Morikawa A, Kawasaki M, et al. Small adenocarcinoma of the lung: histologic characteristics and prognosis. *Cancer*. 1995;75:2844–2852.
25. Yankelevitz DF, Henschke CI. Does 2-year stability imply that pulmonary nodules are benign? *AJR Am J Roentgenol*. 1997;168:325–328.
26. Swensen SJ, Jett JR, Hartman TE, et al. Lung cancer screening with CT: Mayo Clinic experience. *Radiology*. 2003;226:756–761.
27. Benjamin MS, Drucker EA, McLoud TC, et al. Small pulmonary nodules: detection at chest CT and outcome. *Radiology*. 2003;226:489–493.
28. Hasegawa M, Sone S, Takashima S, et al. Growth rate of small lung cancers detected on mass CT screening. *Br J Radiol*. 2000;73:1252–1259.
29. Nakata M, Sawada S, Saeki H, et al. Prospective study of thoracoscopic limited resection for ground-glass opacity selected by computed tomography. *Ann Thorac Surg*. 2003;75:1601–1606.
30. Suzuki K, Yokose T, Yoshida J, et al. Prognostic significance of the size of central fibrosis in peripheral adenocarcinoma of the lung. *Ann Thorac Surg*. 2000;69:893–897.
31. Aoki T, Tomoda Y, Watanabe H, et al. Peripheral lung adenocarcinoma: correlation of thin-section CT findings with histologic prognostic factors and survival. *Radiology*. 2001;220:803–809.
32. Yankelevitz Df, Reeves AP, Kostis WJ, et al. Small pulmonary nodules: volumetrically determined growth rates based on CT evaluation. *Radiology*. 2000;217:251–256.
33. Ko JP, Rusinek H, Jacobs EL, et al. Small pulmonary nodules: volume measurement at chest CT-phantom study. *Radiology*. 2003;228:864–870.

13-143-4　経尿道的前立腺切除術のための管状組織低侵襲切除マニピュレータ

A Tubular Organ Resection Manipulator for Transurethral Resection of the Prostate

○橋本 隆二　金 大永　波多 伸彦　土肥 健純

東京大学 情報理工学系研究科 知能機械情報学専攻

Ryuji Hashimoto, Daeyoung Kim, Nobuhiko Hata and Takeyoshi Dohi

Dept. of Mechano-Informatics, The University of Tokyo

1. 背景

前立腺肥大症は高齢男性に頻度の高い症例のひとつであり，おもな症状に夜間頻尿・排尿刺激症があげられる[1]．

現在治療法として経尿道的前立腺切除術（Transurethral Resection of the Prostate, TUR-P）が一般的に行われている．これは電気メスと内視鏡を内装した切除鏡を経尿道的に挿入し，内視鏡画像の下，肥大前立腺を切除する手技である．開腹手術に代わる低侵襲な手技とされているが，尿道粘膜の損傷による尿路感染，長時間の手術による TUR 症候群などの合併症が問題視されている[2]．さらに TUR-P では内視鏡の一画像のみで手技を行うため，前立腺と電気メスの位置関係の把握が困難であり，前立腺被膜穿孔や腹腔内穿孔などの合併症を起こす可能性が高い．

これらの合併症を導く問題点を解決するため多くのデバイスが提案されてきたが[3-9]，これらを同時に解決する切除手法および切除デバイスは報告されていない．そこで本研究の目的は，尿道粘膜の損傷を抑え短時間で多くの前立腺組織を取り除く機構を有した，管状組織低侵襲切除マニピュレータの開発である．また画像誘導システムを開発し，安全に切除を行うシステムを構築する．

2. 管状組織低侵襲切除法

2. 1 屈曲切除機構および灌流切除機構

尿道粘膜の損傷を抑え切除を行う機構として，屈曲切除機構を考案した（Fig. 1）．マニピュレータ先端部にはアームとカッターが装備されている．先端部を経尿道的に挿入し，前立腺目的位置まで挿入した後バルーンカテーテルを膨らませ位置固定を行う．アームを屈曲させ患部組織を変位させ，その後カッターを直線的に挿入することで切除を行う．アームの屈曲角度とカッターの挿入量を変化させることで，一点の切開部を通じて広範囲の肥大前立腺組織を切除することが可能となる．また，一平面内の切除が完成した後，先端部を軸方向に回転させることにより，他平面内の肥大組織の切除が可能となり，これらの自由度によって 3 次元的に低侵襲な切除をすることができる．

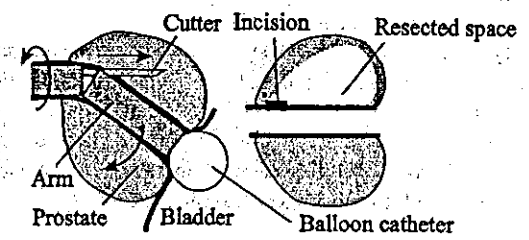

Fig.1 Prostate displacement mechanism

またカッター内部にはドリルと灌流管を内装してあり，カッターが患部に挿入されるとドリルが回転し組織を切削，ローラポンプにより灌流液を流し込み，切除片と灌流液を同時に体外に取り除く．切除と吸引を同時に行うため短時間の切除が可能となる．

2. 2 システム全体像

システム構成を Fig.2 に示す．本システムはマニピュレータ・術者操縦用コントローラ・画像誘導システムの 3 つからなる．始めにマニピュレータを経尿道的に患部に挿入し，マニピュレータを保持しているポイントセッターを固定する．術者は画像誘導を下にコントローラを操作し，マニピュレータを操縦し切除を行う．術者を誘導する画像には超音波画像を用いる．患部とマニピュレータ先端部を撮像し，術者に両者の位置関係を把握させ安全な切除を行わせる．

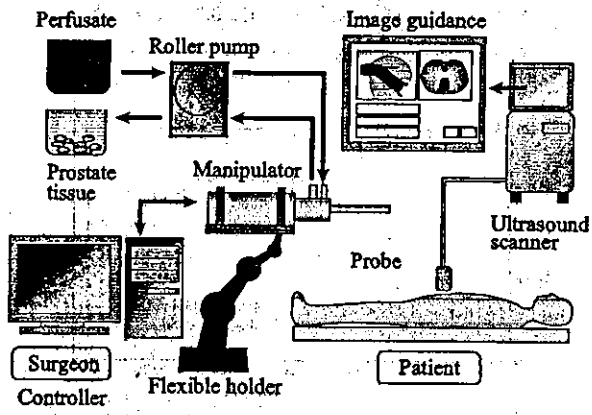

Fig.2 Conceptual model of the complete system

2. 3 マニピュレータ詳細

製作したマニピュレータの先端部を Fig. 3 に示す．マニピュレータ先端はアーム・カッター・ドリルを持つ．搭載された自由度は 4 自由度であり，アームの屈曲・カッターの挿入・ドリルの回転・軸周りの回転を有する．

先端部の大きさは直径 8mm であり，従来用いられている切除鏡の直径に等しい．アームの屈曲にはリンク屈曲機構を用い，確実な前立腺の屈曲を実現できる．アーム屈曲角度は最大 45°，分解能は 0.1° である．前立腺尿道部は人によって長さが異なるため，アームの長さはこれに対応できるよう可変となっている．写真では 40mm の長さのアームを取り付けてある．カッターの挿入ストロークは最大 40mm，分解能 0.1mm，本体軸方向の回転は ±180° である．

第 2 回生活支援工学系学会連合大会（２００４年９月、東京）

マニピュレータ先端部は臨床での有用性を考慮し，全て分解・滅菌可能であり，かつ本体駆動部に取り付け具なしで取り付けられる機構になっている．

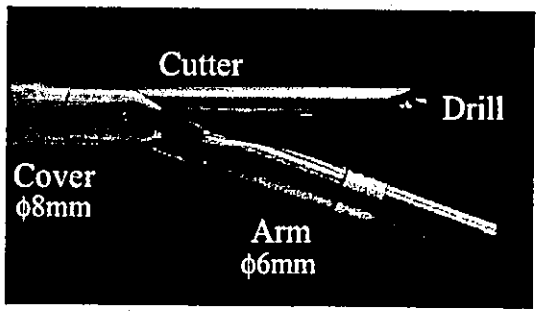

Fig.3 Endeffector of the manipulator

3. 評価実験

3. 1 屈曲特性評価

前立腺屈曲のための先端部アームは，先端にかかる負荷によって特性が異なることが予備実験によりわかっている．従って，先端に負荷を加えた状態でのアームの屈曲特性を評価した．アーム先端に，50gfずつ荷重を加えていき，マニピュレータに 25° 屈曲する指令を送り，実際に屈曲する角度を測定した．屈曲特性の結果をFig. 4 に示す．

アームの屈曲角度は，負荷を大きくするほど指令値に対し出力値が小さくなることがわかった．最大誤差は負荷が300gfの時であり，その値は6.3° であった．また屈曲のばらつきに関しては標準偏差の平均は0.7° であった．

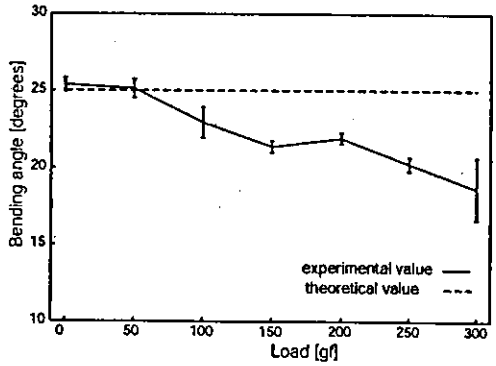

Fig.4 Bending characteristics of the arm with loaded condition

3. 2 ファントム実験

前立腺のファントムとしてゼラチンを用い，屈曲および切除実験を行った．前立腺尿道部 45mm，肥大前立腺外径50mmの円柱型ゼラチンモデルに，尿道にあたる直径 4mmの空洞をつくり，これにマニピュレータ先端部を挿入し，屈曲・切除を行った．ファントム実験の屈曲・切除の様子をFig.5 に，切除したモデルの断面形状をFig.6 に示す．

切除の手順は以下の通りである．マニピュレータを経尿道的に挿入し，始めにアームを 45° 屈曲させ，カッターを 40mm 挿入し切除吸引を行った．その後アームの角度を5° 戻す度にカッターを挿入し，切除吸引を行った．

評価項目は，1 平面内の切除における切除範囲と，挿入口の損傷の大きさを測定した．

1 平面切除における平均切除面積は 65.3mm^2 であり，カッター挿入部の大きさの平均は直径 3.8mm であった．

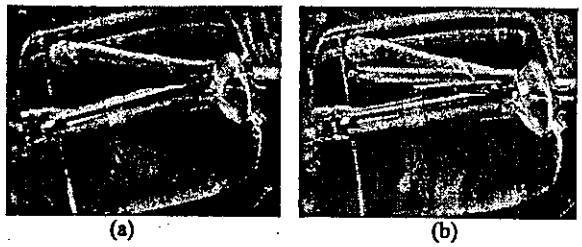

(a) (b)

Fig.5 Resection procedure: (a) Cutter insertion at bending angle 30° (b) Cutter insertion at bending angle 15°

Fig.6 Cross section of gelatin model after resection

4. 考察

負荷を与えたアームの屈曲特性は，負荷の大きさに伴い屈曲角度が小さくなった．屈曲機構で用いるリンクの変形が最も大きく影響を与えていると考えられる．しかしどの負荷においても 1° 以下の再現性が得られているため，荷重・実測値をもとに屈曲角度の補正をすることが可能である．

ファントム実験においては，アームが組織を確実に変位させることができること，3.8mm の小孔から非常に広い範囲の組織を切除・吸引できることがわかった．今後はより肥大前立腺組織に近いファントムを用い，本機構の有用性を評価していく．

5. まとめ

本研究では経尿道的前立腺切除術のための管状組織低侵襲切除マニピュレータを開発した．屈曲切除機構と灌流切除機構により低侵襲な切除と，短時間での切除を実現した．

参考文献

1. S. J. Berry, *et al*, The Development of Human Benign Prostatic Hyperplasia with Age, Journal of Urology, **132(3)**, pp474-479, 1984

2. K. Koshiba, *et al*, Does Transurethral Resection of the Prostate Pose a Risk to Life – 22year Outcome, Journal of Urology, **153(3)**, pp1506-1509, 1995

3. Q. Mei, *et al*, PROBOT – A Computer Integrated Prostatectomy System, Visualization in Biomedical Computing, **1311**, pp581-590, 1996

4. K. Matsumiya, *et al*, A New Robotic Device for Less Invasive Transurethral Resection of the Prostate, Computer Assisted Radiology and Surgery, pp134-138, 2000

SP2-I: Medical Robotics II

Room I, 16:10-17:30, Saturday, October 2, 2004

SP2-I1 16:10-16:30

Development of SPINEBOT for Spine Surgery

G.B. Chung, S.G. Lee, S.M. Oh, B.-J. Yi, W. K. Kim, Y.S. Kim, J.I. Park, and S.H. Oh
Center for Intelligent Surgery System, Hanyang University, KOREA

- The surgical procedure for spinal operation and possible roles of the robot are discussed.
- The expected simplest role of SPINEBOT is to provide the guide to locate and orient the surgical tools more accurately.
- The tracking experiment to compensate for the respiratory movement of the human body is conducted by using optical tracking system.
- The interaction force between the end-effector of SPINEBOT and the mockup vertebra is measured to verify the applicability of SPINEBOT to tasks of boring and inserting screws automatically.

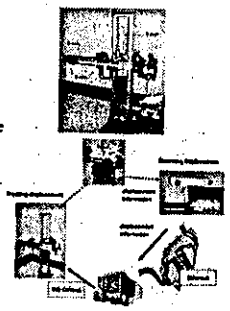

SP2-I2 16:30-16:50

A new mechanical birth simulator : BirthSIM

R. Silveira, O. Dupuis, M.T. Pham, T. Redarce, M. Bétemps
Institut National des Sciences Appliquées de Lyon - France
Hôpital de la Croix Rousse Lyon - France

BirthSIM is a complete system for training and testing new techniques in obstetric practice. It is composed of three parts:

- a physical new-born head and a maternal pelvis manikin,
- an interface pressure system,
- a pneumatic actuator that develops an active resistance.

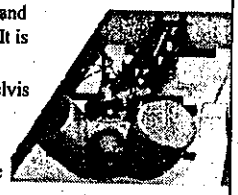

BirthSIM

Driven by a computer, **BirthSIM** can simulate the contractions and mimic birth complications.

SP2-I3 16:50-17:10

A Tubular Organ Resection Manipulator for Transurethral Resection of the Prostate

Ryuji Hashimoto Dayoung Kim Nobuhiko Hata Takeyoshi Dohi
Graduate School of Information Science and Technology
The University of Tokyo, JAPAN

- The manipulator realizes less invasive resection of the prostate for TUR-P surgery
- Two novel mechanisms:
  - Prostate displacement mechanism
  - Perfusion-resection mechanism
- Description of manipulator design
- Accuracy evaluation & Phantom study

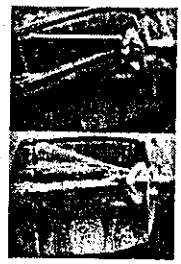

SP2-I4 17:10-17:30

Palpation Instrument for Augmented Minimally Invasive Surgery

Maria Vatshaug Ottermo, Øyvind Stavdahl and Tor A. Johansen
Norwegian University of Science and Technology, Norway

- A preliminary design of a remote palpation instrument for Minimally Invasive Surgery with tactile feedback
- A piezoelectric sensor array attached to the instrument's end effector will provide tactile information
- The sensor array is 24*8 mm² and consists of 30 sensors
- The tactile information will be sent to surgeon's fingers via a tactile display
- The tactile display is 32*18*45 mm³ and consists of 30 micro motors

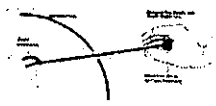

A sketch of the instrument with tactile sensor and display

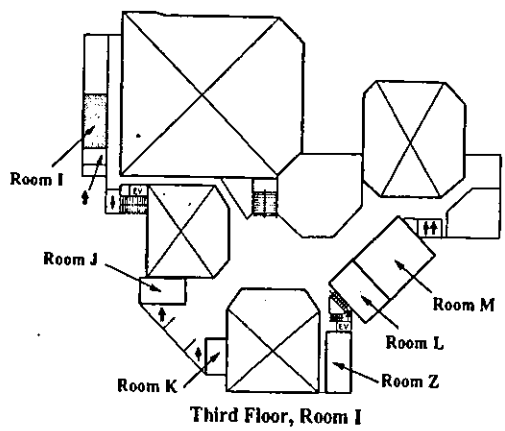

Third Floor, Room I

Proceedings of 2004 IEEE/RSJ International Conference on
Intelligent Robots and Systems
September 28 - October 2, 2004, Sendai, Japan

A Tubular Organ Resection Manipulator for Transurethral Resection of the Prostate

Ryuji Hashimoto Daeyoung Kim Nobuhiko Hata Takeyoshi Dohi
Department of Mechano-Informatics, Graduate School of Information Science
The University of Tokyo
7-3-1 Hongo, Bunkyo-Ku, Tokyo, 113-8656, Japan
Email:{hashimoto, young, noby, dohi}@atre.t.u-tokyo.ac.jp

Abstract—**Transurethral resection of the prostate (TUR-P) is a common treatment for Benign Prostatic Hyperplasia (BPH). However, the damage to the mucous membrane of the urethra leads to the complications. This paper reports a tubular organ resection manipulator for transurethral resection of the prostate which can minimize damage to the mucous membrane of the urethra using a prostate displacement mechanism and a continuous perfusion-resection mechanism. The manipulator has an arm, a cutter and a drill at the endeffector, and has 4 degrees-of-freedom: bending the arm, translating the cutter, rotating the drill and rotating the endeffector. The arm displaces the prostate, and the cutter is inserted linearly into the prostate and removes enlarged tissue by drilling. Combination of the arm and cutter enables the manipulator to remove sufficient volume of enlarged prostate through small incision on the urethra, thus minimizing the damage to the urethra. After finishing one plane cutting, the manipulator rotates its body and removes another part of the prostate gland. In performance experiments, each mechanism (bending motion, insertion, and body rotation) had high repeatability within 1.0 degree and within 0.1 mm. In phantom study, the manipulator could displace gelatin model accurately with sufficient power, and could reach and remove wide range of sample tissue (589.2 mm^2 in one procedure). These results showed that the manipulator can displace the prostate and remove sufficient volume of the prostate tissue through small incision on the urethra.**

I. Introduction

Benign prostatic hyperplasia (BPH) is a noncancerous enlargement of the prostate gland. As a man ages, the prostate becomes enlarged and places pressure on the urethra. This leads to urination trouble and dysfunction of the bladder and kidney. More than half of all men in their 60s, and as many as 80 percent of men in their 70s and 80s, have some symptoms of BPH [1], [2].

Transurethral resection of the prostate (TUR-P) is currently standard method of cure for BPH. As compared with the conventional open surgery, TUR-P has advantages such as less invasive and shorter hospitalization. In the TUR-P procedure, the surgeon inserts a resectoscope through the urethra, and cuts the prostate tissue into small pieces with an electrical loop during the 90-minute operation. The resected tissue are carried by the perfusate into the bladder and then flushed out at the end of the operation. After surgery, the removed tissue is routinely checked for hidden cancer cells [3], [4].

However, some complications are possible with TUR-P procedure. Urinary tract infection (UTI) occurs with damage to the mucous membrane of the urethra during tissue resection of an enlarged prostate. TUR syndrome, which leads to dizziness and nausea, occurs with absorption of perfusate in extended surgery. TUR-P procedure by nature is difficult procedure for physicians due to limited view of surgical field in resectoscope (Fig. 1). This leads to the perforation of the prostate capsule, resulting in rectal injury or bladder damage [5], [6], [7].

Some devices have been proposed by several groups to avoid the TUR-P complications. Davies developed a PROBOT for TUR-P surgery under accurate control, with guidance provided by a 3D model of the prostate generated from the ultrasound images [8], [9]. Accurate and repeatable cutting by the manipulator realizes safe cutting of the prostate, and prevents bleeding and damage to sphincter muscle and nerves. Matsumiya has proposed a preliminary design for a prostatectomy cutter which reaches the prostate via a small incision on the urethra [10]. These devices have possibility of reducing some complications. However, no device has focused on above two complications; UTI and TUR syndrome which is the serious problems in TUR-P procedure, and no device has reported that can both minimize the damage to the urethra, and remove enlarged prostate in short time.

As a solution for these problems, we reported a transurethral prostate resection manipulator which can prevent the damage to the urethra and remove sufficient volume of the prostate in short time [11]. In previous study, the prototype had three degrees-of-freedom and could not complete whole range resection. Furthermore we had to develop the whole system such as a controller for surgeon, and image guidance for safe resection. The objectives of the current study are to complete the further degree-of-freedom of the manipulator, and to confirm feasibility of proposed prostatectomy. This paper reports 1) description of the newly developed tubular organ resection manipulator, 2) its mechanical performance analysis and 3) results of phantom experiment using a gelatin model to evaluate usefulness of less invasive resection mechanism.

II. Prostate Displacement Mechanism

A. System Requirement

In order to overcome the complications of TUR-P procedure, detailed requirements for the manipulator system is summarized as follows:

0-7803-8463-6/04/$20.00 ©2004 IEEE

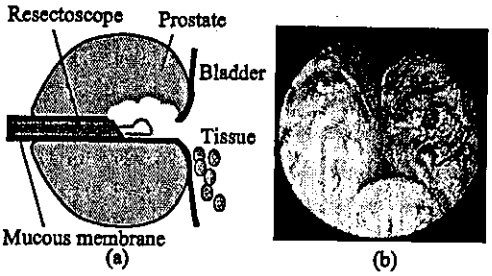

Fig. 1. Conventional resection procedure of TUR-P. The problems of TUR-P procedure is 1) damage to the mucous membrane of the urethra (a), 2) absorption of perfusate in extended surgery and 3) deep cutting due to limited view in resectoscope (b).

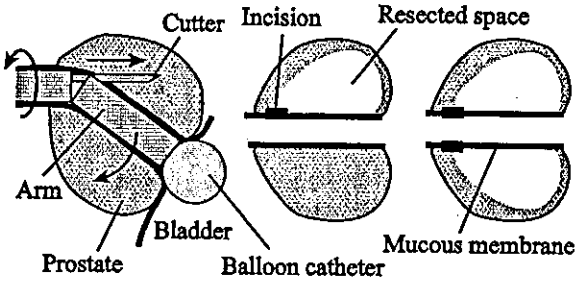

Fig. 2. Prostate displacement mechanism for minimizing damage to the mucous membrane. The end effector of the manipulator has the arm and cutter. Combination of the arm and cutter enable the manipulator to resect sufficient volume of the prostate tissue through small incision.

- The manipulator should remove the tissue through small incision on the urethra.
- The manipulator should remove sufficient volume of the tissue in short time.
- The system should provide enough image information which surgeon can grasp position between the end effector and the target tissue.
- The end effector of the manipulator should be small enough to be inserted through urethra, and be demountable and sterilizable.

Based on these system requirements, we proposed two novel mechanisms and resection system described below.

B. Prostate displacement mechanism

Figure 2 shows the prostate displacement mechanism to prevent damage to the mucous membrane of the urethra. End effector of the manipulator has an arm and a cutter. Firstly, the manipulator is inserted through the urethra. Then the arm bends to displace the enlarged prostate, and the cutter is inserted into the prostate to remove prostate tissue by cutting.

While the cutter cuts the enlarged tissue moving only linearly, the arm can change its angle. Thus the possibility of incision in the mucous membrane can be restricted to a single point.

Organs such as the bladder and sphincter muscle are situated around the prostate, and should not be damaged. We thus attach a balloon catheter to the end of the arm.

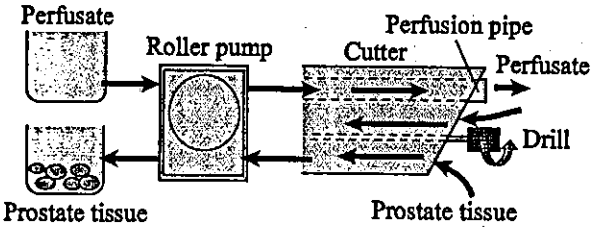

Fig. 3. Continuous perfusion-resection mechanism for rapid resection. Roller pump inlet the perfusate into the prostate through perfusion pipe, then the drill cut the prostate tissue, then the pump aspirate the prostate tissue and perfusate as fluid outside of the body.

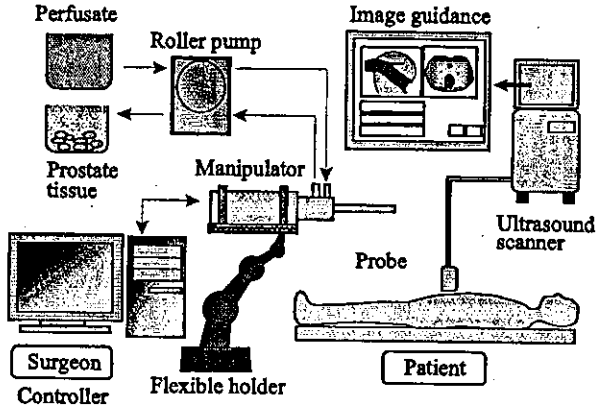

Fig. 4. Conceptual model of the complete system. The system consists of three parts; a manipulator, an image-guided system and controller. The surgeon controls the manipulator from the controller and resects the prostate tissue while watching the multi slice images from the image-guided system.

When the balloon is inflated, it holds the manipulator steady against the urethra, and keeps the position between the manipulator and the prostate, thus preventing damage to these organs.

C. Continuous perfusion-resection mechanism

Figure 3 shows the continuous perfusion-resection mechanism for rapid resection. The cutter is equipped with a drill and a perfusion pipe. While the cutter is inserted into the prostate, the drill continues to cut the enlarged tissue into small piece by rotating. A roller pump inlet perfusate into the prostate through the perfusion pipe; the perfusate is mixed with the prostate tissue and is removed outside the body by the roller pump. Using this mechanism, the manipulator can cut and remove the enlarged tissue at the same time, thus realizing a short time resection.

III. System Configuration

The system has three parts: a manipulator, an image-guided system, and a controller (Fig. 4). The manipulator is fixed to a flexible holder (Point Setter, Mitaka Kouki Inc., Japan). Firstly, the manipulator is inserted into the prostate through the urethra. The flexible holder is then locked, and the surgeon controls the manipulator using a controller under the ultrasound guidance. We use a transrectal or

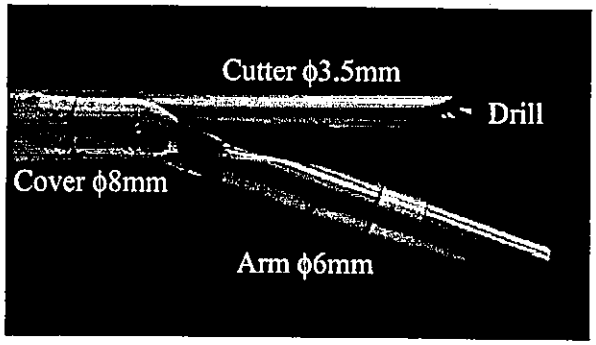

Fig. 5. End effector of the manipulator has the arm, cutter and drill. The end effector has 4 degree-of-freedom; 1) bending the arm, 2) translating the cutter, 3) rotating the drill and 4) rotating the end effector.

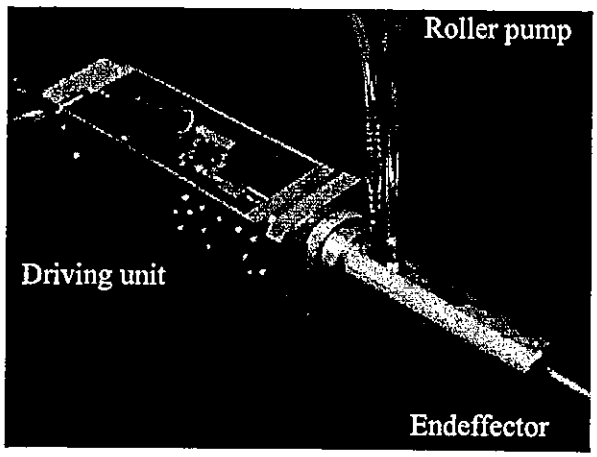

Fig. 6. Driving unit of the manipulator. Driving unit has four motors, three photo sensors and two ball screws, and delivers generation power to the end effector. Connection mechanism realizes quick connection between the driving unit and the end effector.

transabdominal ultrasound probe (EUP-C514 EUP-CC531, Hitachi Medical Co., Japan) for image guiding. Ultrasound device (EUB-525, Hitachi Medical Co., Japan) provides the multi slice imaging of the prostate. Using US guidance, the surgeon can easily grasp the position between the end effector and prostate and the other organs. Thus the possibility of unexpected damage to the prostate capsule or the bladder neck can be reduced. These devices realize a minimally invasive, efficient and safe resection.

A. Manipulator Specification

We developed the tubular organ resection manipulator. The manipulator consists of an end effector and a driving unit.

1) 4 Degrees-of-freedom end effector: Figure 5 shows the end effector which has 4 degree-of-freedom: 1) bending of the arm, 2) translating of the cutter, 3) rotating the drill and 4) rotating the end effector. The arm is 6 mm in diameter and 40-mm in length. The arm can change its angle range of 0 to 45 degrees, with a resolution of 0.1 degrees. Length of the arm can be changed 20 to 50 mm because length of intraprostatic urethra varies by patients.

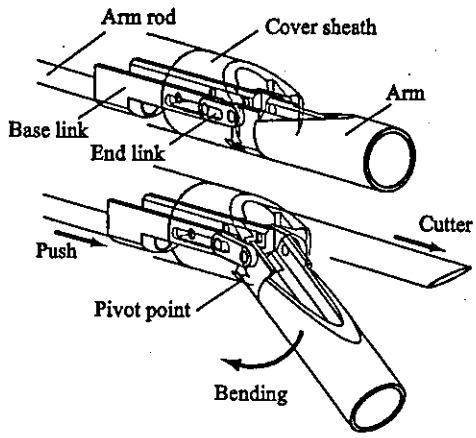

Fig. 7. Slider linkage mechanism consists of cover sheath, arm rod, base link, end link and arm. The actuator pushes the arm rod, and then base link transmit its power to the end link, then the end link bends the arm around its pivot point.

The diameter of the cutter is 3.5 mm. Its stroke length is 40 mm, with a resolution of 0.1 mm. The diameter of the cover sheath, which is inserted in the urethra, is 8 mm. This is the same size as the resectoscope. The manipulator can rotate its end effector range of -180 to 180 degrees. These elements are demountable and sterilizable. Using these 4 degrees-of-freedom, the end effector can remove sufficient volume of prostate tissue through small incision on the urethra.

The driving unit consists of motors, photo-sensors and ball screws. The rotational velocity and direction of the motor is controlled from a console. The ball screws transform rotation of the motors into translation. The photo-sensors are used to tune the zero-point of the arm and cutter. These elements are unsterilizable, so the driving unit has to be covered by a drape during the operation. The size of the driving unit is 50×65×235 mm.

2) Displacement and Perfusion-resection mechanism: In order to displace the enlarged prostate accurately, we adopted a slider linkage mechanism for bending (Fig. 7), because it realizes greater stiffness and fewer backlashes than a wire-driven system. When the actuator pushes or pulls a base link, the end link bends or extends the arm around its pivot point. Figure 8 shows a working space of the arm. Combination of arm bending and body rotation, the arm can reach whole range of the enlarged prostate model.

Figure 9 shows the detail of the continuous perfusion-resection mechanism. The mechanism consists of perfusion pipe (0.5 mm in outer diameter) and drill (2.4 mm in diameter). The roller pump inlet the perfusate into the prostate through the perfusion pipe, then drill cuts the prostate tissue into small pieces, and the pump aspirates the tissue and perfusate through another port of the cutter. Output pressure of the roller pump is 200 kPa and maximum flow rate of the perfusate is 90 ml/min. This mechanism realizes a short time resection.